Energy Advances

ROYAL SOCIETY OF CHEMISTRY

PAPER

View Article Online
View Journal | View Issue

Cite this: *Energy Adv.*, 2024, 3, 2212

Enhancing the solid-state hydrogen storage properties of lithium hydride through thermodynamic tuning with porous silicon nanowires

Rama Chandra Muduli, †[a] Zhiwen Chen,†[b] Fangqin Guo, *[b] Ankur Jain, [d] Hiroki Miyaoka,[c] Takayuki Ichikawa [b] and Paresh Kale *[a]

Received 20th June 2024,
Accepted 14th July 2024

DOI: 10.1039/d4ya00389f

rsc.li/energy-advances

Solid-state hydrogen storage technology ensures a safer storage method, eliminating the risks of leaks, boiling losses, and explosions in commercial applications. Based on earlier findings, alloying LiH with silicon (Si) yields substantial storage capacity while lowering the energy needed for absorption and decomposition. Herein, the work explores using the derivative of bulk Si (*i.e.*, porous silicon nanowires (PSiNWs)) after mechanical milling with LiH to improve the thermodynamic properties and uptake capacity. The PSiNWs are synthesized by Ag metal-assisted chemical etching of the bulk Si substrate. Nanopores on the nanowires enhance gas physisorption by overlapping attractive fields from opposing pore walls. The large surface area (~450 m^2 g^{-1}) of the PSiNWs provides maximum active sites for hydrogen storage. The hydrogen storage capacity of the LiH–PSiNW alloy is evaluated through pressure composition isotherms at different temperatures (400–500 °C range) and ~4 MPa charging pressure. The maximum observed capacity, ~3.95 wt%, occurs at 400 °C. The thermodynamic analysis signifies the uniform absorption and desorption enthalpy after alloying LiH with PSiNWs. Hydrogen absorption and desorption enthalpies of ~118 kJ mol^{-1} H_2 and ~115 kJ mol^{-1} H_2 demonstrate a reduced energy requirement compared to individual LiH. The phase formation and variations before and after hydrogenation are studied by X-ray diffraction. This work investigates using Si nanostructures and light metal hydrides for enhanced hydrogen storage and cyclic functionalities, serving as both a storage material and catalyst.

1. Introduction

The global energy demand experienced significant growth and is projected to increase by ~75% between 2000 and 2030.[1] Current commercial fossil fuel energy sources harm the environment, causing irreversible damage to our earth. Hydrogen is a desirable fuel with a high gravimetric energy density (higher and lower heat values: ~142 kJ g^{-1} and ~120 kJ g^{-1} H_2) and a potential substitute for fossil fuels, offering a clean and carbon-neutral energy source for a sustainable society.[2] However, safe and reliable storage are major challenges after hydrogen production. Thus, research on storage and transportation is ongoing to find efficient and cost-effective hydrogen utilization methods. Temperature and pressure tuning for safety concerns, but with considerable gravimetric energy density, are key advantages of storing hydrogen in materials. Metal hydride-based hydrogen storage offers superior energy density and safety compared to conventional storage methods.[3,4] Fast kinetics, good reversibility, and low-pressure storage (≤1 MPa) are significant advantages of metal hydrides for hydrogen storage.[5]

Lithium (Li) is a popular light energy storage material with a maximum theoretical energy density of ~2 kW h kg^{-1} and 1 kW h L^{-1}.[6,7] Li and hydrogen form light metal hydrides with an equivalent energy density of ~5 kW h kg^{-1} and 3.9 kW h L^{-1}.[8] Releasing hydrogen from LiH requires high temperatures (~900 °C for 0.1 MPa),[9] posing a significant challenge for its reversible storage applications despite its high theoretical capacity (~12.6 wt%) for hydrogen storage.[3,10] The estimated enthalpy of hydride decomposition is ~181 kJ mol^{-1} H_2, which proves to be economically unviable for cyclic energy storage. Additionally,

[a] *Department of Electrical Engineering, National Institute of Technology Rourkela, 769008, Odisha, India. E-mail: muduliramachandra@gmail.com, pareshkale@nitrkl.ac.in*
[b] *Graduate School of Advanced Science and Engineering, Hiroshima University, 1-4-1 Kagamiyama, Higashi-Hiroshima 739-8527, Japan. E-mail: d216356@hiroshima-u.ac.jp, fang-qin-guo@hiroshima-u.ac.jp, tichi@hiroshima-u.ac.jp*
[c] *Natural Science Center for Basic Research & Development, Hiroshima University, 1-3-1 Kagamiyama, Higashi-Hiroshima 739-8530, Japan. E-mail: miyaoka@hiroshima-u.ac.jp*
[d] *Centre for Renewable Energy & Storage, Suresh Gyan Vihar University, Jaipur, 302017, India. E-mail: ankur.j.ankur@gmail.com*
† Contributed equally.

the limited diffusion of hydrogen within LiH results in sluggish kinetics, leading to a prolonged duration for the reaction to reach completion.

The thermodynamic tuning of LiH for cyclic hydrogen storage involves combining it with other hydrogen storage materials.[3] Previously, rare work on LiH alloys with Mg,[11] fullerene,[12] graphite,[8] Ge,[13] Sn,[14] and Ni[15] was reported for reversible hydrogen storage. However, achieving substantial thermodynamic tuning and ensuring sufficient hydrogen storage capacity remain essential for cyclic application. Destabilization of LiH was conducted (electrochemical study) by group 14 elements, suggesting a stable nature of the Li–M alloy (M = Group 14 elements, *i.e.*, C, Si, Ge, and Sn) compared to pure Li.[8,12–14,16] Jain *et al.*[13] concluded that Si is the optimized destabilizing element, keeping a balance between the operating temperature (400 °C to 500 °C) and reversible hydrogen storage capacity (~4 wt%). Bulk Si faces challenges due to its low surface area and limited volumetric storage capacity, highlighting the need for improvements to enhance its energy storage properties.

Silicon nanostructures (SiNSs) exhibit extensive surface area, substantial porosity, and heightened surface energy, facilitating the presence of numerous active sites that effectively attract hydrogen.[2,17] A previous investigation examined the morphology and absorption–desorption properties of silicon nanostructures (SiNSs), including porous silicon (PS), silicon nanowires (SiNWs), and porous silicon nanowires (PSiNWs), for hydrogen storage purposes.[17,18] PS and PSiNWs possess significant potential to adsorb hydrogen at lower adsorption and decomposition energy.[17,19] In the past, PS was combined with LiH to enhance the thermodynamic properties and enable the absorption of ~3.1 wt% of hydrogen at 400 °C and 1 MPa.[3] The absorption and desorption behavior improves with the increase in the nanopores in the storage materials. Nanopores on the nanowires enhance gas sorption by attractive fields from opposing pore walls to overlap.[2,17] The rough surface and large surface area (~450 $m^2 g^{-1}$) of PSiNWs provide maximum active sites for hydrogen storage.[17] Still, negligible research was carried out with PSiNWs for hydrogen storage objectives.

This study aims to investigate the synergistic effect of PSiNWs and LiH as alloys on tuning the thermodynamics and hydrogen uptake capacity of LiH. The pressure composition isotherm (PCI) characterizes the hydrogen cyclic behavior and uptake capacity of the LiH–PSiNW alloy at different temperatures (400–500 °C range) at up to ~4 MPa. The thermodynamics governing the absorption and desorption of hydrogen are characterized by the equilibrium reached during the absorption and desorption plateaus. The phases of Li–Si formed during different reaction stages are analyzed using X-ray diffraction (XRD). The novel fusion of a light metal hydride alloyed with PSiNWs in cyclic hydrogen energy storage shows the potential for enabling practical onboard applications.

2. Experimentation and characterization

PS was synthesized by the electrochemical anodization technique on boron-doped, p-type Si wafers (⟨100⟩, 275 ± 25 μm thick, and 0.01–0.02 Ω cm).[18,20] PSiNWs were synthesized on a PS substrate by metal-assisted chemical etching (MACE). The PS substrates were submerged in an electrolyte solution consisting of 0.02 M $AgNO_3$ (supplier: Sigma-Aldrich), 0.1765 M H_2O_2 (supplier: Fisher Scientific), and 4.8 M HF (supplier: Acros Organics) for 60 minutes at ambient temperature. Following the MACE, the synthesized PSiNWs were immersed in deionized water and 30% HNO_3 to eliminate the Ag catalyst from the surface of the nanowires (NWs). An electropolishing technique (100 mA cm^{-2} for 60 seconds) was used to lift off the PSiNW layer from the Si wafer substrate.[17,21] The separated PSiNW films were pulverized into a powder using an agate mortar and pestle. The powdered PSiNWs were heat treated for 1 hour in a reactor (volume of 9.2 cc) under vacuum conditions at 200 °C to eliminate moisture and contaminants, including oxides, hydroxyl, and carboxyl groups.

The mechanical alloying procedure includes blending LiH (supplier: Sigma-Aldrich, purity: 95%) and PSiNWs in a molar ratio of 4.4 : 1. The preparation and handling of the samples were performed within an Ar-filled glove box (Miwa MFG, MDB-2BL). The glove box is outfitted with a recirculation system to maintain the H_2O and O_2 concentrations below 2 ppm and 5 ppm, respectively. The milling procedure was performed at 370 rpm in a 1 bar Argon environment, using the ball milling device (P7, Fritsch) with a 20 cm^3 inner volume (600 mg sample and 20 SUJ-2 balls per jar). The mass ratio of balls to the sample was 52.5 : 1 (*i.e.*, in one jar, 31.5 g balls were used per 0.6 g sample). The process involved three cycles of ball milling, each consisting of one hour of milling followed by a 30-minute resting period to avoid overheating. All chemical handling and alloying processes were conducted inside a glove box flushed with purified argon (99.9999%) to prevent exposure to air. The ball-milled mixed sample was heat treated at 500 °C (for 3 hours) in a reactor under vacuum conditions to prepare the alloy of Li–Si.

Hydrogen storage characteristics were investigated through rate measurements and pressure composition isotherms (PCIs) using a Sievert-type apparatus (maker: Suzuki Shokan Co., Ltd). For the hydrogen storage analysis, 0.5 grams of the LiH–PSiNW alloy sample were taken into a stainless-steel reactor (SUS 316, volume of 9.2 cm^3). The hydrogen gas utilized in the investigation exhibits a purity level of 99.9999%, obtained from Nakamura Sanso Corporation in Japan. The PCI measurements were conducted at five distinct temperatures, ranging from 400 °C to 500 °C, with intervals of 25 °C. The morphologies of the PSiNWs were investigated using scanning electron microscopy (SEM, maker: NOVA NANOSEM 450, FEI, operating voltage = 20 kV). Powder X-ray diffraction measurement (XRD, using the RINT-2500V instrument from Rigaku Corporation, Cu-K_α (λ = 1.54 Å) source, step size = 0.02°, and scan speed = 5° min^{-1}) investigates the phases and crystallinity of the alloys at different stages of reaction. The percentage of the phases involved was calculated using the PDXL software to analyze the XRD patterns.

3. Results and analysis

Fig. 1(a) illustrates the cross-section of the NW array on a PS substrate following the MACE, indicating the fabrication of

NWs elongated to ~4 μm in length. Nanopores are formed on the NW wall due to horizontal etching assisted by Ag^+ ions during MACE in addition to the mesopores in the base (PS).[17,22] The nanopores help to enhance the surface area of the PSiNWs by ~13% from individual PS.[17] The overlapping of potential fields in the PSiNW nanopores may improve the hydrogen uptake capacity.[17,23] Fig. 1(b) illustrates the surface view of PSiNWs, indicating the uniform fabrication of NWs on the PS surface. The PSiNWs are alloyed with LiH by heat-treating at 500 °C for 3 hours, as shown in Fig. 1(c). The particle sizes are not uniform after alloy formation due to the agglomeration and crystallization of particles during heat treatment. Fig. 1(d) illustrates the morphology of the LiH–PSiNW alloy after hydrogen absorption and desorption (PCI cycle) followed by complete desorption (at 500 °C for 1 hour). The particle size reduces after pulverization caused by hydrogenation and dehydrogenation cycles at a charging pressure. Due to the rough surface of the alloyed particles, it seems like the broccoli structure with high surface energy attracts hydrogen (refer to the magnified images in Fig. 1(c) and (d)). The hydrogen absorption and desorption behavior are further discussed using PCI measurements.

The PCI measurement for hydrogen absorption of the LiH–PSiNW alloy at varying temperatures within the range from 400 °C to 500 °C is shown in Fig. 2(a), demonstrating the absorption thermodynamic behavior of hydrogen. The α, α + β, and β phases signify the initial bulk absorption of hydrogen, formation of ionic hydrides, and hydrogen saturation exceeding the equilibrium pressure (P_{eq}), respectively. During the α + β phase, an average absorption of approximately 1.5 wt% is observed, with lower pressure plateaus ranging from 0.01 to 0.1 MPa. Considering the maximum charging pressure of up to ~4 MPa, the hydrogen uptake capacity is maximum (~3.95 wt%) at 400 °C. The range of α + β phase is maximum with a slanting β phase for absorption at 400 °C, indicating an increased uptake capacity compared to other temperatures. The possible reason is the activation of the nano and mesopores within the PSiNWs at a lower temperature of 400 °C, along with hydrogen entrapment at the Li–Si interface.

The relation between the equilibrium pressure (P_{eq}) and the enthalpy changes (ΔH) and entropy (ΔS) provides the thermodynamic parameters for hydrogen absorption and desorption in the alloy using the van't Hoff equation (eqn (1)).[3] The P_{eq} is determined by considering the midpoint of the plateau. R is the ideal gas constant, and T is the material hydrogen absorption temperature. The slope and intercept of the graph represent the values for enthalpy and entropy, respectively, as obtained from Fig. 2(b). The hydrogenation enthalpy and entropy are 118.1 ± 7.48 kJ mol^{-1} H_2 and 139.2 ± 10.47 J mol^{-1} K^{-1} H_2,

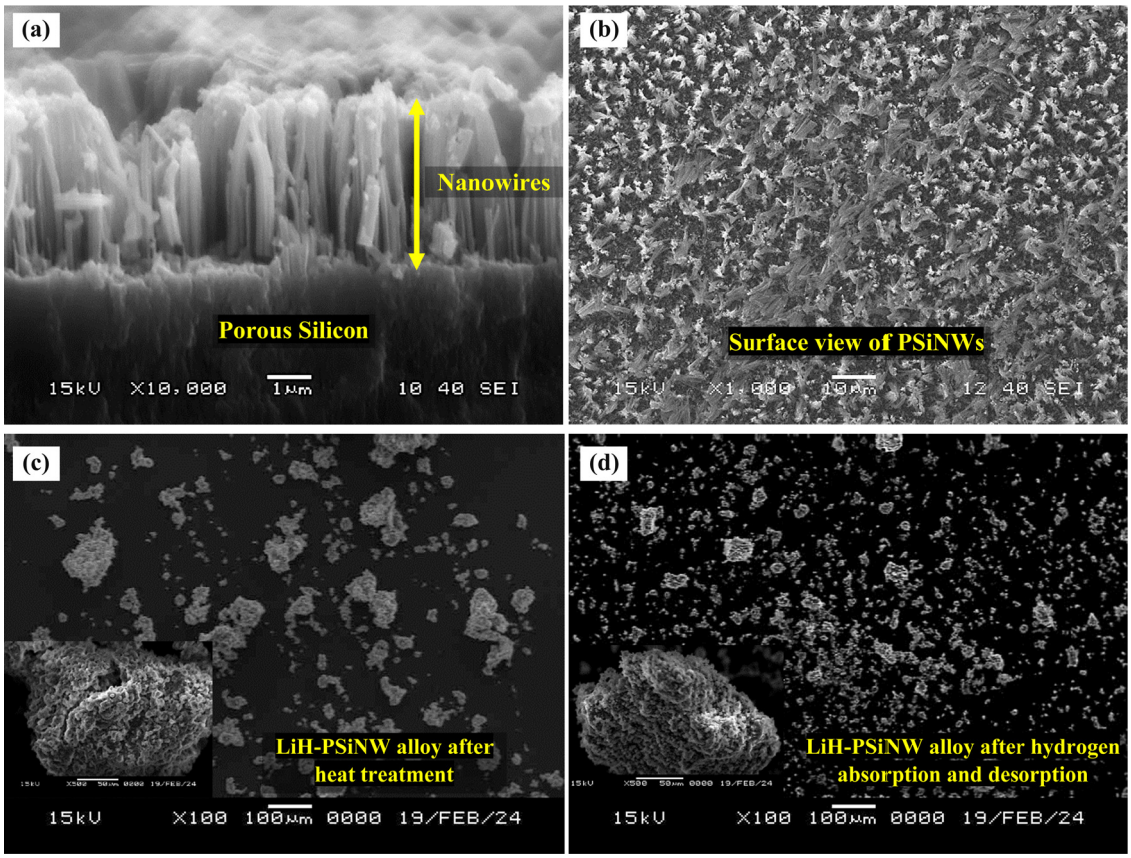

Fig. 1 Scanning electron microscopy of (a) the cross-section of the PSiNWs after electrochemical anodization, (b) surface view of the SiNWs, (c) LiH–PSiNWs after alloy formation, and (d) LiH–PSiNWs followed by hydrogen desorption (500 °C for 1 hour) after PCT.

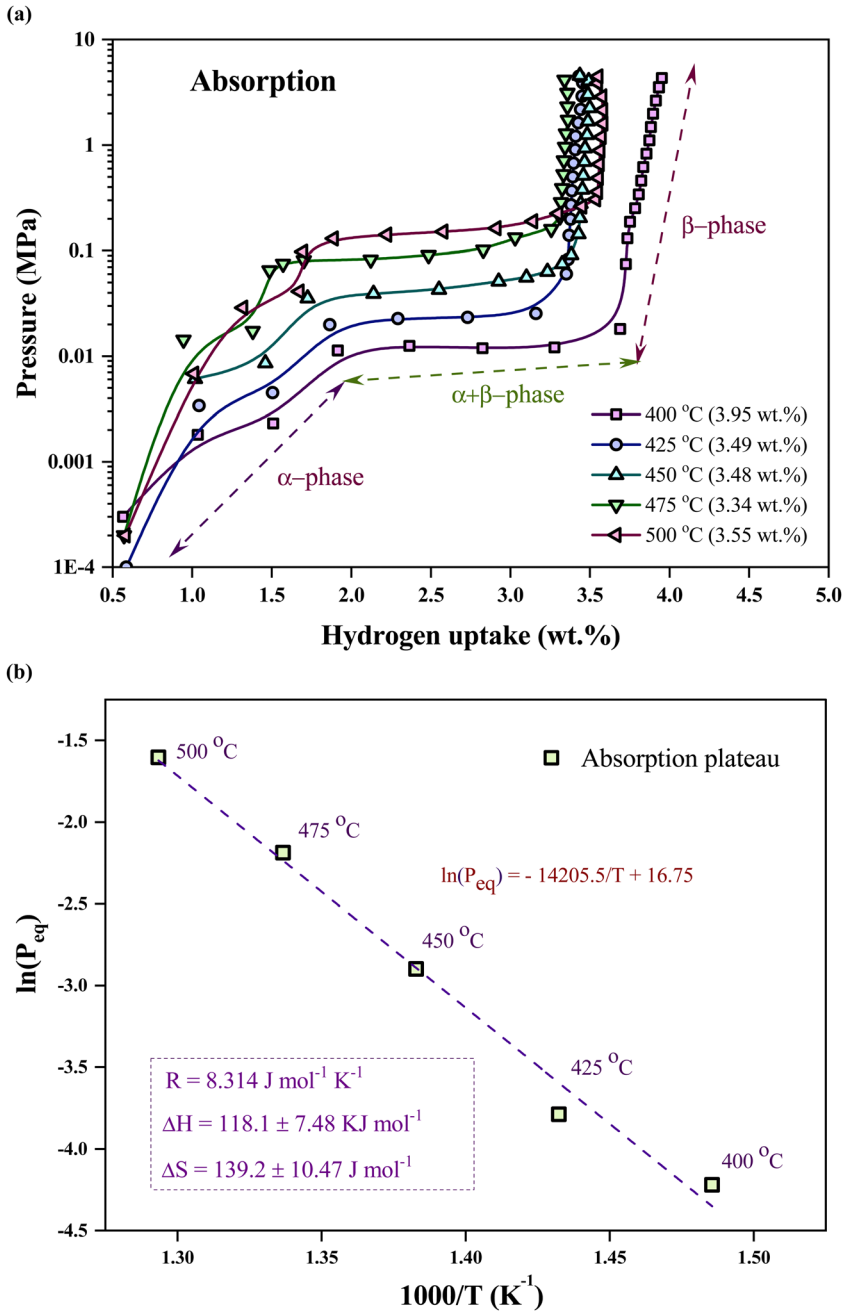

Fig. 2 Pressure composition isotherm of the LiH–PSiNW alloy: (a) hydrogen absorption and (b) desorption at 400 °C, 425 °C, 450 °C, 475 °C, and 500 °C.

respectively. The magnitude of enthalpy is lower than the formation energy required for hydride formation with Li (*i.e.*, ~180 kJ mol^{-1}).

van't Hoff equation:

$$\ln\left(\frac{P_{eq}}{P_o}\right) = \left(\frac{\Delta H}{R}\right)\frac{1}{T} - \frac{\Delta S}{R} \quad (1)$$

The disparity in reaction enthalpies corresponds to absorption and desorption, leading to the parallel desorption path (hysteresis) observed in the PCI profiles (refer to Fig. 3(a)). In the desorption process, the plateaus align parallelly with the absorption plateau, indicating that hydrogen is uniformly released at the related temperature with decreasing pressure.[18] The difference in absorption and desorption plateau is due to the lattice strain and mechanical difference between metal and metal hydride structures. Multiple phases and phase transformations within the alloy result in a double desorption plateau.

The van't Hoff plot concerning the two desorption plateaus (as shown in Fig. 3(b)) yields enthalpy values of 115.5 ± 2.2 kJ mol^{-1} and 118.4 ± 2.23 kJ mol^{-1} for the lower and higher desorption

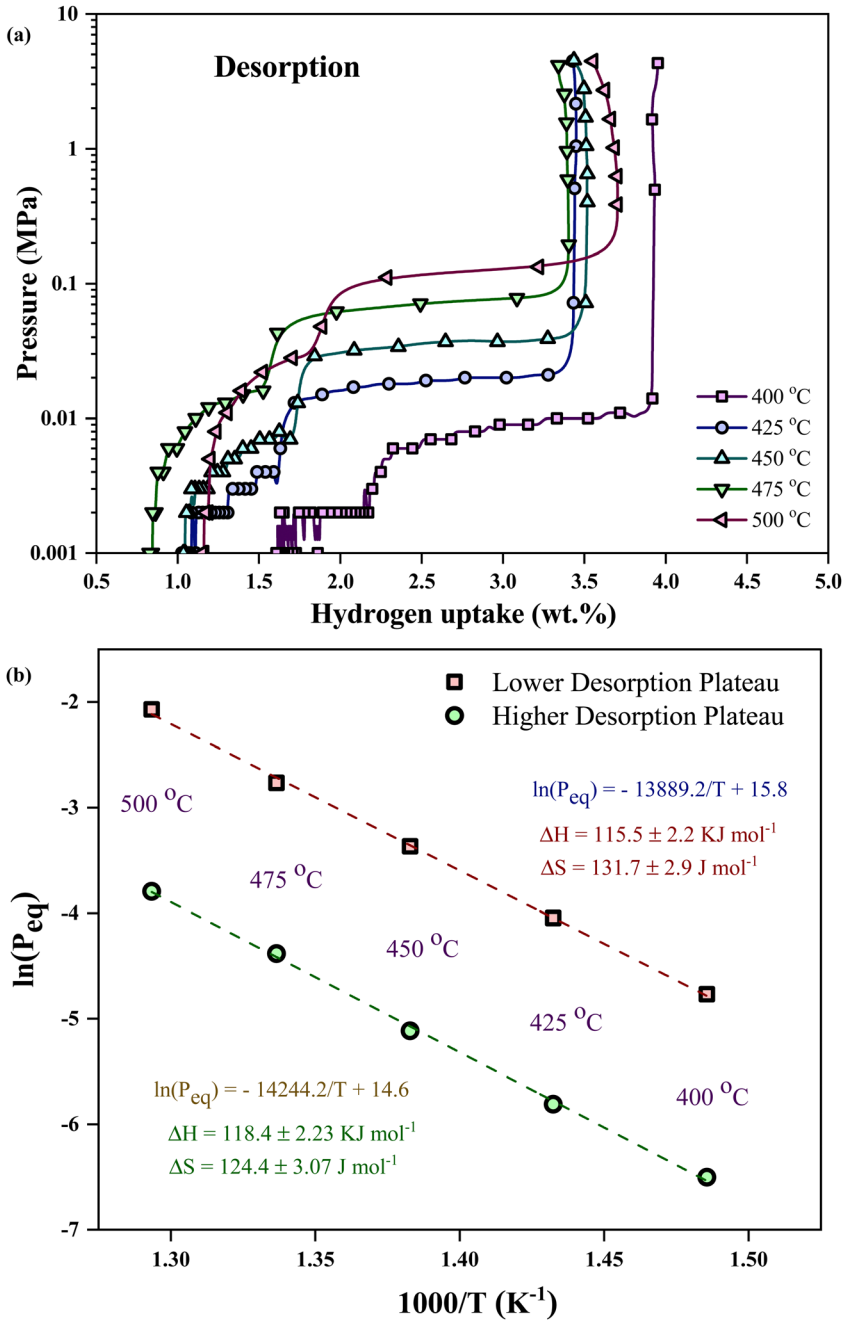

Fig. 3 (a) PCI desorption isotherm of the LiH–PSiNW alloy at 400 °C to 500 °C with 25 °C temperature interval and (b) van't Hoff plot for hydrogen desorption at lower and higher desorption plateau pressure regions.

plateau pressures, respectively. The endothermic desorption reaction for hydride decomposition from the alloy results in a positive change in enthalpy. The endothermic desorption process may be impacted by the mixed phases involved or changes in volume caused by phase shifts.[3] Desorption from the α + β phase and the α-phase regions is the potential reason for higher and lower plateau pressures. The XRD profile indicates the possible phase distribution at different stages of thermal treatments and hydrogen absorption–desorption of the alloy.

Following ball milling and 3 hours of heat treatment at 500 °C, the XRD pattern of the LiH–PSiNW alloy (refer to Fig. 4) indicates $Li_{13}Si_4$ as the primary phase, alongside minor phases like Li_7Si_3, Li_2O, and LiH. It is noted that the existence of Li_2O suggests that LiH is highly reactive and prone to oxidation, even in the glovebox environment (O_2 < 5 ppm). After the hydrogenation of the alloy, the phases change to LiH and Si due to the ionic reaction of hydrogen with Li. After one cycle of hydrogen absorption and desorption in PCI, $Li_{12}Si_7$ emerges as the predominant phase, accompanied by a minor presence of LiH. The recyclability of the alloy is determined by the re-emergence of Li–Si phases from LiH upon dehydrogenation. The hydrogenated alloy dehydrogenates through heat

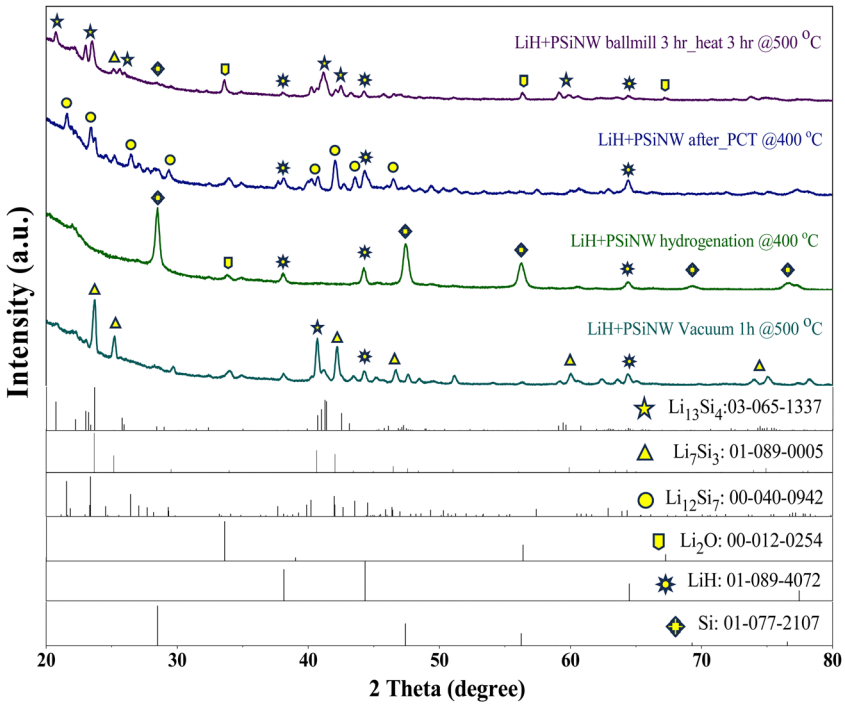

Fig. 4 XRD analytical technique of the LiH–PSiNW alloy at four different stages (peaks of concerned phases are leveled): after ball milling followed by 3 hours of heat treatment at 500 °C for alloy formation, after the PCT cycle at the optimized temperature (400 °C), after hydrogenation at 400 °C, and followed by hydrogen desorption (500 °C for 1 hour) after PCT (400 °C).

treatment at 500 °C for one hour. The dominant phase transitions to Li_7Si_3, with $Li_{13}Si_4$ and LiH as minor phases. The proportions of the phases were determined through analysis of the XRD patterns using PDXL software, as listed in Table 1.

4. Discussion

The work investigates the effect of PSiNWs on LiH in tuning the thermodynamic properties for hydrogen absorption and desorption. The large surface area of $\sim$400 m^2 g^{-1} [17] provides high surface energy to form alloys with LiH, and the nanopores attract hydrogen to react with the material. Due to the activation of PSiNWs and dangling sites, the hydrogen uptake capacity is enhanced at lower temperatures (400 °C), as discussed in PCI. Both lower saturation pressure and high uptake capacity are observed at 400 °C, indicating an optimized temperature for the alloy for hydrogen cyclic storage. The parallel desorption plateaus observed during desorption suggest uniform hydrogen release at the corresponding temperatures as pressure decreases. The enthalpy value indicates the demand for hydrogen absorption and desorption at a lower pressure and higher temperature. The isosteric heat (Q_{st}) of absorption reflects the potential energy needed as the uptake capacity and pressure increase.

Q_{st} provides information about the affinity between the sorbate gas and the sorbent substrate.[3,24] The Clausius–Clapeyron equation (referred to as eqn (2)) calculates the absolute absorption enthalpy (ΔH) at a constant level of hydrogen uptake (wt%) for each absorption temperature. The slope (η) of the ln P *versus* $1/T$ plot is ΔH, and the absolute value of ΔH is referred to as the Q_{st}. Fig. 5 illustrates the Q_{st} value plotted relative to the quantity of hydrogen absorption, with delineation among three temperature limit zones for absorption (namely, higher temperature zone: 450–500 °C, all temperature, and lower temperature zone: 400–450 °C). In the initial absorption phase (α-phase) of higher and lower temperature zones, the absorption energy indicates the dominance of Li and PSiNWs, respectively. Considering all the absorption temperatures, the behavior results from higher and lower energy zones. Chemisorption resulting from the ionic absorption of Li occurs in the α + β phase region, resulting in nearly uniform energy requirements across all

Table 1 Possible percentage of phase formation at various stages of alloy

Various stages of alloys	$Li_{13}Si_4$	Li_7Si_3	$Li_{12}Si_7$	Li_2Si	Li_2O	Si	LiH
3 h ball milled LiH + PSiNW heat at 500 °C for 3 h	65.0	7.8			14.6		13.6
LiH + PSiNW hydrogenation at 400 °C					3.8	31.2	65.0
LiH + PSiNW vacuum at 500 °C for 1 h	25.0	59.0					16.0
LiH + PSiNW after PCT@400 °C			50.5	4.5			45.0

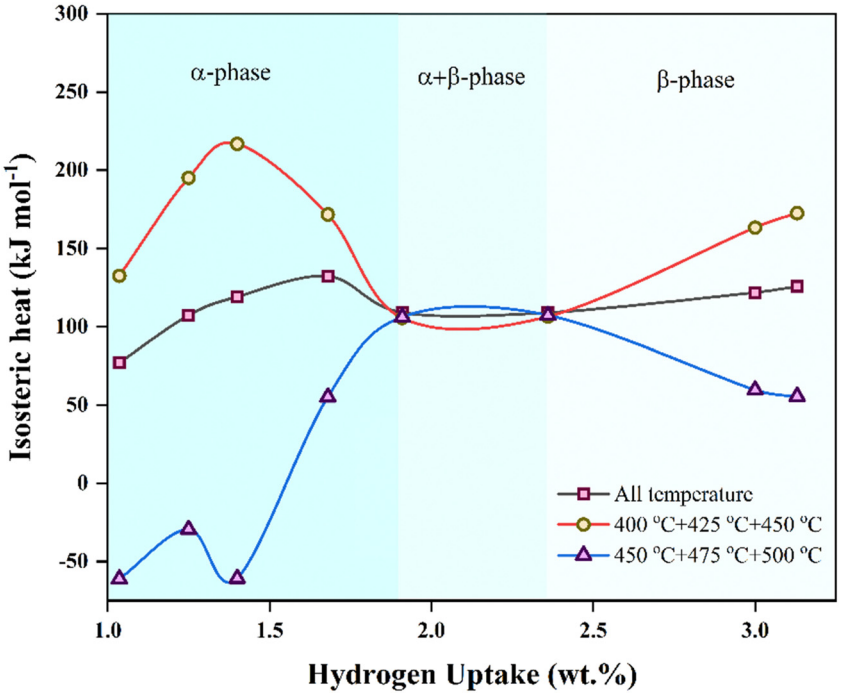

Fig. 5 Isosteric heat of hydrogen absorption (Q_{st}) as a function of hydrogen uptake for the LiH–PSiNW alloy at different temperature zones.

zones. In the uptake saturation zone (β phase), the behavior of Q_{st} follows the same as in the α-phase. In the uptake saturation zone (β phase), the Q_{st} behavior parallels as observed in the α-phase. An energy requirement below 100 kJ mol^{-1} in the lower temperature zone (*i.e.*, <450 °C) with an uptake capacity ≥ 3.5 wt% indicates the suitability of the LiH storage alloy material compared to most previously reported LiH alloys.[11–14,25]

Clausius–Clapeyron equation:

$$Q_{st} = -R\left[\frac{\partial \ln P}{\partial(1/T)}\right]_{wt\%} = -R\eta \quad (2)$$

The XRD profile confirms the dominant phases of $Li_{13}Si_4$ ($Li_{3.25}Si$), $Li_{12}Si_7$ ($Li_{1.71}Si$), and Li_7Si_3 ($Li_{2.33}Si$) in the sample of LiH–PSiNW mixture heated at 500 °C for 3 h, the sample of LiH–PSiNW after one cycle of PCI and the sample of dehydrogenated LiH–PSiNW mixture at 500 °C for 1 h after PCI, respectively. The possible reversible hydrogenation reaction with each phase is illustrated in eqn (3)–(5).

$$Li_{3.25}Si + 1.625H_2 \leftrightarrow Si + 3.25LiH \quad (3)$$

$$Li_{1.71}Si + 0.855H_2 \leftrightarrow Si + 1.7LiH \quad (4)$$

$$Li_{2.33}Si + 1.165H_2 \leftrightarrow Si + 2.33LiH \quad (5)$$

The ionic hydride formation with Li after hydrogenation and phase transformation after dehydrogenation indicates the possibility of reversible hydrogen storage in the alloy. The current industrial synthesis of LiH from lithium and hydrogen necessitates either 700 °C at atmospheric pressure or a hydrogen pressure of 50 MPa at ambient temperature.[8] This study facilitates the thermodynamic tuning of LiH by alloying with PSiNWs, which reduced the operating temperature to below 450 °C.

5. Conclusions

The study examines the primary constraints associated with individual lithium for hydrogen absorption and desorption, which include its high thermodynamic stability. Using mechanical milling, LiH was alloyed with PSiNWs in a molar ratio of 4.4 : 1. The hydrogen absorption and desorption were measured at varying temperatures from 400 °C to 500 °C. The hydrogen uptake capacity is 3.95 wt% at ~4 MPa and 400 °C. The absorption (118.1 ± 7.48 kJ mol^{-1} H_2) and desorption (115.5 ± 2.2 kJ mol^{-1} H_2) enthalpy indicate a lower energy requirement for cyclic storage than individual LiH and most used metal hydrides. The isosteric heat of absorption validates the role of PSiNWs in thermodynamically tuning LiH and suggests 400 °C as the optimal temperature for cyclic hydrogen storage. The hydride formation from the Li–Si alloyed phase after hydrogenation and *vice versa* after dehydrogenation indicates the potential for cyclic utilization of the alloy.

Data availability

The manuscript represents all the data acquired in the work as graphs and tables. No data is shared with any repository or cloud storage.

Conflicts of interest

There are no conflicts to declare.

Acknowledgements

This research is part of a collaborative project funded by the Department of Science and Technology (DST/INT/JSPS/P-353/2022 (G), 19th September 2022) in India and the JSPS Joint Research Project (JPJSBP120227715) in Japan. The authors sincerely appreciate the financial support extended by both organizations.

References

1 D. Gielen, F. Boshell, D. Saygin, M. D. Bazilian, N. Wagner and R. Gorini, The role of renewable energy in the global energy transformation, *Energy Strategy Rev.*, 2019, **24**, 38–50, DOI: 10.1016/j.esr.2019.01.006.

2 R. Chandra Muduli and P. Kale, Silicon nanostructures for solid-state hydrogen storage: A review, *Int. J. Hydrogen Energy*, 2023, **48**, 1401–1439, DOI: 10.1016/j.ijhydene.2022.10.055.

3 R. Chandra Muduli, Z. Chen, K. Shinzato, F. Guo, T. Ichikawa and A. Jain, *et al.*, Thermodynamic improvement of lithium hydrides for hydrogen absorption and desorption by incorporation of porous silicon, *Int. J. Hydrogen Energy*, 2023, **50**, 1094, DOI: 10.1016/j.ijhydene.2023.09.015.

4 J. Andersson and S. Grönkvist, Large-scale storage of hydrogen, *Int. J. Hydrogen Energy*, 2019, **44**, 11901–11919, DOI: 10.1016/j.ijhydene.2019.03.063.

5 R. Napán, Y. Peltzer and E. L. Blancá, First-principles studies of lithium hydride series for hydrogen storage, *Int. J. Hydrogen Energy*, 2012, **37**, 5784–5789, DOI: 10.1016/j.ijhydene.2011.12.117.

6 J. Wang, Y. Li and X. Sun, Challenges and opportunities of nanostructured materials for aprotic rechargeable lithium-air batteries, *Nano Energy*, 2013, **2**, 443–467, DOI: 10.1016/j.nanoen.2012.11.014.

7 X. B. Cheng, J. Q. Huang, Q. Zhang, H. J. Peng, M. Q. Zhao and F. Wei, Aligned carbon nanotube/sulfur composite cathodes with high sulfur content for lithium-sulfur batteries, *Nano Energy*, 2014, **4**, 65–72, DOI: 10.1016/j.nanoen.2013.12.013.

8 L. Wang, M. Z. Quadir and K. F. Aguey-Zinsou, Direct and reversible hydrogen storage of lithium hydride (LiH) nanoconfined in high surface area graphite, *Int. J. Hydrogen Energy*, 2016, **41**, 18088–18094, DOI: 10.1016/j.ijhydene.2016.07.073.

9 A. Jain, E. Kawasako, H. Miyaoka, T. Ma, S. Isobe and T. Ichikawa, *et al.*, Destabilization of LiH by Li insertion into Ge, *J. Phys. Chem. C*, 2013, **117**, 5650–5657, DOI: 10.1021/jp400133t.

10 S. Banger, V. Nayak and U. P. Verma, Hydrogen storage in lithium hydride: A theoretical approach, *J. Phys. Chem. Solids*, 2018, **115**, 6–17, DOI: 10.1016/j.jpcs.2017.11.027.

11 M. Pęska, T. Czujko and M. Polański, Hydrogenation ability of Mg-Li alloys, *Energies*, 2020, **13**, 2080, DOI: 10.3390/en13082080.

12 J. A. Teprovich, M. S. Wellons, R. Lascola, S. J. Hwang, P. A. Ward and R. N. Compton, *et al.*, Synthesis and characterization of a lithium-doped fullerane (Li x-C 60-H y) for reversible hydrogen storage, *Nano Lett.*, 2012, **12**, 582–589, DOI: 10.1021/nl203045v.

13 A. Jain, H. Miyaoka and T. Ichikawa, Destabilization of lithium hydride by the substitution of group 14 elements: A review, *Int. J. Hydrogen Energy*, 2016, **41**, 5969–5978, DOI: 10.1016/j.ijhydene.2016.02.069.

14 A. Jain, H. Miyaoka, T. Ichikawa and Y. Kojima, Correlation between electrochemical behavior and hydrogen storage properties of Li-Sn system, *J. Alloys Compd.*, 2013, **580**, S211, DOI: 10.1016/j.jallcom.2013.03.150.

15 L. Wang, M. Z. Quadir and K. F. Aguey-Zinsou, Ni coated LiH nanoparticles for reversible hydrogen storage, *Int. J. Hydrogen Energy*, 2016, **41**, 6376, DOI: 10.1016/j.ijhydene.2016.01.173.

16 M. Yoshio, H. Wang, K. Fukuda, T. Umeno, T. Abe and Z. Ogumi, Improvement of natural graphite as a lithium-ion battery anode material, from raw flake to carbon-coated sphere, *J. Mater. Chem.*, 2004, **14**, 1754–1758, DOI: 10.1039/b316702j.

17 R. Chandra Muduli and P. Kale, Chemically modified surface of silicon nanostructures to enhance hydrogen uptake capabilities, *Int. J. Hydrogen Energy*, 2022, **48**, 37819–37833, DOI: 10.1016/j.ijhydene.2022.06.030.

18 R. C. Muduli, N. Gupta, P. Sharma and P. Kale, Investigating reversible hydrogen storage and performance of porous Si by kinetic study and pressure composition isotherms at up to 20 bar, *Int. J. Hydrogen Energy*, 2024, **59**, 447–456, DOI: 10.1016/j.ijhydene.2024.01.156.

19 R. C. Muduli and P. Kale, Synergetic effect of porous silicon–Nickel composite on its solid-state hydrogen energy storage properties, *Int. J. Hydrogen Energy*, 2023, **48**, 35185–35196, DOI: 10.1016/j.ijhydene.2023.05.268.

20 V. K. Hiremath, R. C. Muduli and P. Kale, Investigation of the Stability and Insulating Properties of Mineral Oil-Based Surface Modified Silicon Nanofluid, *IEEE Trans. Dielectr. Electr. Insul.*, 2023, 1, DOI: 10.1109/TDEI.2023.3242231.

21 S. P. Muduli and P. Kale, Free-standing nanowire layer-transfer parametric optimisation of multi-response process by Grey Taguchi design, *Mater. Sci. Technol.*, 2022, **39**(5), 591–599, DOI: 10.1080/02670836.2022.2129203.

22 D. Jung, S. G. Cho, T. Moon and H. Sohn, Fabrication and characterization of porous silicon nanowires, *Electron. Mater. Lett.*, 2016, **12**, 17–23, DOI: 10.1007/s13391-015-5409-y.

23 S. Li, W. Ma, Y. Zhou, X. Chen, Y. Xiao and M. Ma, *et al.*, Fabrication of porous silicon nanowires by MACE method in HF/H2O2/AgNO3 system at room temperature, *Nanoscale Res. Lett.*, 2014, **9**, 1–8, DOI: 10.1186/1556-276X-9-196.

24 S. S. Samantaray, V. Sangeetha, S. Abinaya and S. Ramaprabhu, Diatom frustule-graphene based nanomaterial for room temperature hydrogen storage, *Int. J. Hydrogen Energy*, 2020, **45**, 764–773, DOI: 10.1016/j.ijhydene.2019.10.155.

25 A. Huq, J. W. Richardson, E. R. Maxey, D. Chandra and W. M. Chien, Structural studies of Li3N using neutron powder diffraction, *J. Alloys Compd.*, 2007, **436**, 256–260, DOI: 10.1016/j.jallcom.2006.07.021.